

Second-harmonic generation in dielectric nanoparticles with different symmetries

KRISTINA FRIZYUK,¹

¹*ITMO University, 197101 Saint Petersburg, Russia*
**k.frizyuk@metalab.ifmo.ru*

Abstract: In this work we study second-harmonic generation in a monocrystalline nanoparticle with a non-centrosymmetric crystalline lattice. It was shown that breaking the symmetry of the nanoparticle's shape can significantly affect the second harmonic radiation pattern. We propose a method for explaining and predicting the generated field for arbitrary nanoparticles and provide selection rules for nanoparticles with several different symmetries.

© 2019 Optical Society of America

1. Introduction

Second-harmonic generation (SHG) by resonant nanoparticles has recently been actively studied both theoretically [1–5] and experimentally [6–11] in order to develop nanosized light sources. The absence of phase matching conditions at the subwavelength scales results in significant drop of the generation efficiency, making the exploitation of resonances in such nanoscale structures the only way to enhance SHG. During the last few decades, metallic nanostructures supporting localized surface plasmon resonances have been actively studied — while the lattice of typical plasmonic materials has a center of inversion, second harmonic (SH) generation is still possible by surface and nonlocal volume effects [12–16]. In more recent developments, nanoparticles from dielectrics and semiconductors with a non-centrosymmetric crystalline lattice and bulk second order non-linearity [17–20] have been extensively studied. Mie-resonances supported by these dielectric nanoparticles [21] can lead to several orders of magnitude increase in SHG efficiency compared to metal structures [22]. Despite the large number of studies in this area, the full physical picture explaining SHG enhancement in all-dielectric nanostructures has yet to be identified. Selection rules, i.e. rules that determine the correspondence between the modes excited at the fundamental frequency and the modes at the second harmonic, play one of the most important roles. Selection rules for SHG in nanoparticles from materials that do not have bulk nonlinearity, such as gold, silicon, etc., were studied in detail in [23] for spherical particles, and in [24] for particles of other shapes. Despite the many studies devoted to the investigation of SHG from nanoparticles with bulk nonlinearity, the nature of the multipole composition of the generated fields, as well as the effect of nanoparticle symmetry on it, has not been studied in detail. In most of the works, the results of the SH fields' multipole expansion numerical calculations are presented without an explanation of the physical nature of the appearance of certain modes in the spectrum. The goal of this work is to determine the selection rules for SHG by dielectric nanoparticles with arbitrary symmetries and with a nonlinear susceptibility tensor $\hat{\chi}^{(2)}$. In particular, we will show that a violation of the symmetry can strongly affect the mode composition and, as a result, the radiation pattern of the SH.

2. Derivation of selection rules

According to [21, 25–28], the field \mathbf{E} , which satisfies the Helmholtz equation $\nabla^2 \mathbf{E} + \varepsilon \left(\frac{\omega}{c}\right)^2 \mathbf{E} = 0$ with frequency ω in a medium with dielectric susceptibility ε , can be expanded into a series of vector spherical harmonics $\mathbf{N}_{p,mn}(\sqrt{\varepsilon} \frac{\omega}{c}, \mathbf{r})$ (electric) and $\mathbf{M}_{p,mn}(\sqrt{\varepsilon} \frac{\omega}{c}, \mathbf{r})$ (magnetic), introduced in [21, 29]. They correspond to the electric field of electric and magnetic multipoles of the n th

order.

To make further derivations more compact, the vector spherical harmonics \mathbf{M} and \mathbf{N} will be denoted by the same letter $\mathbf{W}_{p_i p_r mn}(\omega)$, with magnetic harmonics $\mathbf{M}_{p_r mn}$ denoted by index $p_i = (-1)^{n+1}$, and electric harmonics $\mathbf{N}_{p_r mn}$ by $p_i = (-1)^n$. Index n corresponds to the order of the multipole, m takes values from 0 to n , and $p_r = 1$ if the function $\mathbf{W}_{p_i p_r mn}(\omega)$ is even with respect to reflection in the $y = 0$ -plane ($\varphi \rightarrow -\varphi$ in spherical coordinates), and $p_r = -1$ if it is odd. The decomposition of the SH field has the form:

$$\mathbf{E}^{2\omega}(\mathbf{r}) = \sum_{n=1}^{\infty} \sum_{m=0}^n \sum_{p_i, p_r} E_0 [D_{p_i p_r mn} \mathbf{W}_{p_i p_r mn}^{(3)}(2\omega)] \quad (1)$$

The superscript (3) means that the harmonic corresponds to a diverging wave [21]. In [29], using the multipole expansion of the Green's function [28, 30–33] it was shown that the coefficients $D_{p_i p_r mn}$ are proportional to the integral of the scalar product of the induced SH polarization $\mathbf{P}^{2\omega}(\mathbf{r}) = \hat{\chi}^{(2)} \mathbf{E}^{\omega}(\mathbf{r}) \mathbf{E}^{\omega}(\mathbf{r})$ and the vector harmonic with indices p_i, p_r, m, n over the nanoparticle volume:

$$D_{p_i p_r mn} \propto \int_V [\mathbf{W}_{p_i p_r mn}(2\omega) \cdot \hat{\chi}^{(2)} \mathbf{E}^{\omega}(\mathbf{r}) \mathbf{E}^{\omega}(\mathbf{r})] dV. \quad (2)$$

The incident field inside the particle can also be decomposed into vector spherical harmonics [21, 29], where multipolar content depends on the illumination conditions and the nanostructure's symmetry (see, for example, [34]). The contribution of certain multipoles is usually dominant, and due to the possibility of selective excitation, we will separately consider the "overlap integrals" of three multipoles, two of which relate to the incident field. Rewriting the integrand (2) by components and expressing the scalar projections of vector spherical harmonics as scalar products with cartesian basis vectors we show that the generation of the multipole $\mathbf{W}_{p_i p_r mn}$ in the SH from the multipoles $\mathbf{W}_{p'_i p'_r m' n'}$ and $\mathbf{W}_{p''_i p''_r m'' n''}$ in the fundamental mode depends on whether the integrals of the following form vanish:

$$I_{W', W'' \rightarrow W} \propto \chi_{\alpha\beta\gamma}^{(2)} \int_V dV [\mathbf{N}_{\alpha} \cdot \mathbf{W}_{p_i p_r mn}(2\omega)] \times [\mathbf{N}_{\beta} \cdot \mathbf{W}_{p'_i p'_r m' n'}(\omega)] [\mathbf{N}_{\gamma} \cdot \mathbf{W}_{p''_i p''_r m'' n''}(\omega)] \quad (3)$$

Here \mathbf{N}_{α} are basis vectors of the Cartesian coordinate system which are proportional to electric vector harmonics with $n = 1$, taken at zero frequency [29], $\mathbf{N}_x \propto \mathbf{W}_{-1111}(0)$, $\mathbf{N}_y \propto \mathbf{W}_{-1-111}(0)$, $\mathbf{N}_z \propto \mathbf{W}_{-1101}(0)$. Note that summation is performed over repeated indices, and the integral (3) is the sum of the integrals of three scalar products of vector spherical harmonics over all nonzero $\hat{\chi}^{(2)}$ -tensor components.

First, we consider the integrals for the nonzero components of the $\hat{\chi}^{(2)}$ -tensor. According to the selection rule theorem for matrix elements [35], such an integral over the symmetric nanoparticle's volume will be nonzero only if the integrand contains an invariant with respect to all transformations of the particle's symmetry. Since the integrand is a scalar value, it is convenient to expand it in a series in terms of scalar functions $\psi_{p_r mn}(\mathbf{r}, \omega)$: $\psi_{-1 mn}(\mathbf{r}, \omega) = j_n(\sqrt{\epsilon} \frac{\omega}{c} r) \frac{\cos m\phi}{\sin m\phi} P_n^m(\cos \theta)$. Their radial part is invariant with respect to any point transformations, and the angular part is transformed in a known way [36]. Examples of scalar functions that contain invariants with respect to transformations of different particle symmetry groups are shown in Table 1 (first column). These functions contain invariants only if the particle is located in a certain way relative to the coordinate axes. For a particle rotated in an arbitrary fashion, they must be transformed with Wigner D-matrices. In order to understand whether any of the terms of

the integral (3) contain functions invariant with respect to particle symmetry transformations, we first decompose each of the scalar products in functions $\psi_{p_r, mn}(\mathbf{r}, \omega)$ (with $|\mathbf{r}|$ -dependent coefficients). Clebsch-Gordan expansions for scalar products of spherical vectors are known from the literature [37] (7.3.10). Based on them, we obtain the rules that determine the numbers p_r , m , n [29] (Appendix B). These rules are based on the fact that the vector spherical harmonics with the numbers m , n behave in the same way as scalar harmonics under rotations, though, when reflected, the behavior of the magnetic harmonics is opposite. It is also necessary to take into account the orthogonality properties of vector functions, such as: $[\mathbf{N}_{-10n'} \cdot \mathbf{M}_{10n}] = 0$, $[\mathbf{N}_{p_r, mn} \cdot \mathbf{M}_{-p_r, mn}] = 0$. After this procedure, only the sum of the products of three scalar functions remain in the integral $I_{W', W'' \rightarrow W} \propto \chi_{\alpha\beta\gamma}^{(2)} \int_V dV [\sum_{p_r, m, n} c(r) \psi_{p_r, mn}] [\sum_{p'_r, m', n'} c'(r) \psi_{p'_r, m' n'}] \cdot [\sum_{p''_r, m'', n''} c''(r) \psi_{p''_r, m'' n''}]$, and they in turn can be decomposed again into scalar functions with known coefficients [29, 38]: $I_{W', W'' \rightarrow W} \propto \chi_{\alpha\beta\gamma}^{(2)} \int_V dV [\sum_{p_r, m, n} d(r) \psi_{p_r, mn}]$.

In the case of a spherical particle, the integral $I_{W', W'' \rightarrow W}$ can be nonzero only if the coefficient before the ψ_{100} is nonzero. For particles of other symmetries, the presence of the spherically symmetric function ψ_{100} is not necessary, the integral may be nonzero if the decomposition includes at least one of the functions $\psi_{p_r, mn}$ which are invariant with respect to the symmetry transformations of the given particle. This changes the selection rules, for example, the "triangle rule" disappears for all particles except spherical ones.

Table 1 provides simplified selection rules that do not take into account the possible orthogonality of vector functions. The product of the parities $p_i p_r$ as well as the sum of the projections m (the signs \pm can be chosen arbitrarily) of all harmonics under the integral, should give the parities and projections of some functions which are invariant with respect to the particle's group transformations. Due to the form of the integral (3), the unit vectors of the Cartesian coordinate system have indices of vector spherical harmonics with $n = 1$. The corresponding projections in the table are denoted as m^α , $p_r^\alpha p_r^\beta p_r^\gamma = p_r^{\alpha\beta\gamma}$, $p_i^\alpha p_i^\beta p_i^\gamma = -1$. The table shows that the lower the symmetry of a particle, the weaker the selection rules for SHG. However, it can be seen that for a cylinder lying on its side, the rules look "weaker" than for a cylinder oriented along the z -axis. This is due to the fact that selection rules don't provide the exact form of the coefficients before each multipole. For example, the function ψ_{102} , which is invariant for the z -oriented cylinder, is presented as a sum of the functions $\psi_{p_r, m2}$ when rotated [36, 39], so, for the arbitrarily oriented cylinder the specific combination of $\psi_{p_r, m2}$ is invariant, while the selection rules can't specify it (see Fig. 1). Because of this, it is advisable to choose the most natural location of the coordinate system, which will reveal a greater number of forbidden transitions. When we choose an arbitrary coordinate system, the multipoles with all possible m and p_r appear in a generated field, but they are still the multipoles with specific m and p_r , but rotated with help of Wigner D-matrixes. For a similar reason, selection rules at the bottom of table 1 look different for different orientations of the prism or pyramid, but these are the same rules in different coordinate systems.

$$\Psi_{102}^{rot} \sim d_{102} \Psi_{102} + d_{122} \Psi_{122}$$

Figure 1. Transformation of spherical function under rotation

The SHG from structures with Td lattice ($\chi_{\alpha\beta\gamma} = \chi |\epsilon_{\alpha\beta\gamma}|$, ϵ – Levi-Chivita tensor), especially AlGaAs or GaAs nanostructures, is extensively studied [6, 40, 41], and interesting properties of

the SH signal revealed [42,43], so, on the right side of table 1 we illustrate the selection rules with the example of such structures. We depict the radiation patterns of allowed multipoles generated by the x -polarized plane wave, whose \mathbf{E} -field is even under $y = 0$ -plane reflection ($p'_r = p''_r = 1$), and $m'^{\omega} = m''^{\omega} = 1$ [21]. Crystalline axes [001], [010], [100] are oriented along the coordinate system axes, so in such material $p_r^{\alpha\beta\gamma} = -1, \pm m^{\alpha} \pm m^{\beta} \pm m^{\gamma} = 0, \pm 2$. Applying the rules for a z -oriented cylinder, we should take $p_r = -1$ and $m^{2\omega} = 0, 2, 4$ to get the invariant functions $\psi_{10(2z)}$ under the integral (3). Radiation patterns of some multipoles with these numbers are provided in the table. When we reduce the symmetry of a structure, additional multipoles become allowed, examples of their appearance are shown in comparison with a higher-symmetry cylindrical structure. The plane wave has low symmetry itself, so the differences between different structures are not very strong, sometimes appearing only for high multipolar orders. However, the contributions of the multipoles are defined by the resonances of the structure, and sometimes it's reasonable to consider only major contributions to the fundamental wave, which makes the rules more specific. We consider an example of a single-mode excitation in the next section. Note that if we change the orientation of the crystalline lattice or excitation wave, the corresponding indexes will change and it is necessary to apply the rules again.

Although the rules given in the table allow a large number of forbidden transitions to be detected, sometimes it is necessary to decompose the integrand over scalar functions for each of the $\hat{\chi}$ -component, as described in [29], to obtain more strict selection rules. This still does not exclude the existence of specific prohibitions, for example, due to integration over the radius. However, if we pay attention to the properties of the tensor $\hat{\chi}^{(2)}$ during the crystalline lattice's group transformations, we can extract additional information about the selection rules in the system. So far, the obtained rules applied to each of the addends in (3) separately, however, after summing up over the repeated indices α, β, γ , additional restrictions may appear due to the fact that the addends mutually destroy each other because of lattice symmetry. The method of detecting these prohibitions is based on the fact that under symmetry transformations, which are common elements of particle's and lattice's groups, (the mutual orientation of the lattice and the particle is important) the intergral (3) must be invariant as a whole. Indeed, under transformations from the crystalline lattice's group, the tensor $\hat{\chi}^{(2)}$ is not transformed, and only three vector harmonics are transformed, which means that for the integral over the particle volume to be nonzero, the product $\mathbf{W}_{p'_i p'_r m'' n''}(\omega) \otimes \mathbf{W}_{p'_i p'_r m' n'}(\omega) \otimes \mathbf{W}_{p_i p_r m n}(2\omega)$ should contain an invariant for all particle transformations that do not change the tensor $\hat{\chi}^{(2)}$. Thus, it is necessary to consider the behavior of vector harmonics with respect to the intersection of the particle's and lattice's groups, and to determine whether their product contains an invariant representation. Symmetry classification and irreducible representations of vector spherical harmonics for finite groups are given, for example, in [29,44].

3. Single-mode excitation

According to [45,46], selective excitation of individual multipoles at the fundamental frequency is possible. Therefore, for simplicity, we consider SHG by a magnetic dipole \mathbf{M}_{-101} (parallel to the z -axis) in a monocrystalline nanocylinder (Fig. 2) from gallium arsenide (T_d lattice, $\varepsilon = 12.96$, with the crystal axes directed along the coordinate axes). A similar geometry was studied experimentally in [47]. To study the effect of symmetry breaking, a cylinder truncated along the $x = y$ plane was also considered. The wavelength corresponding to the fundamental frequency ω is 1480 nm, the cylinder's radius is 140 nm, and it's height is 280 nm. The smallest width of the truncated cylinder is 230 nm. We computed the SH radiation patterns with COMSOL Multiphysics for both nanoparticles. The calculations show that for the whole cylinder the main share of the radiation is accounted for the magnetic quadrupole (\mathbf{M}_{-122}), and negligibly small for higher-order multipoles, since the frequency is far from their resonances. In the case of symmetry breaking (truncated cylinder), the generation of the electric dipole along the z -axis

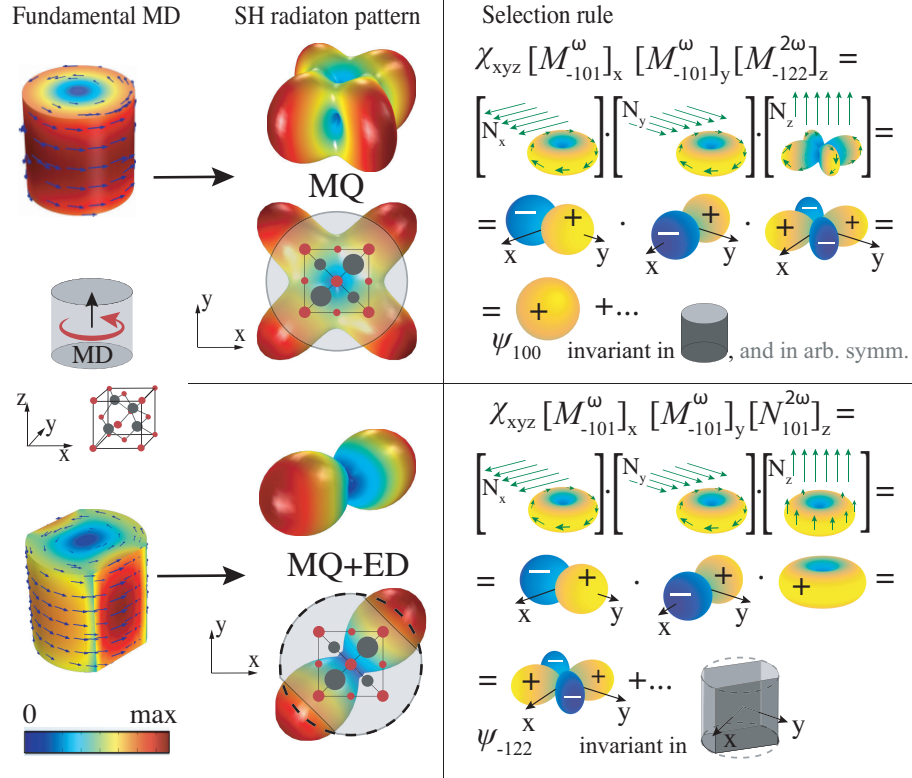


Figure 2. Second-harmonic radiation patterns generated by a magnetic dipole (MD) at the fundamental frequency for the GaAs cylinder (top left), and the GaAs cylinder truncated laterally along the plane $x = y$ (bottom left). For the cylinder, the main generated mode is the magnetic quadrupole (MQ). In the truncated cylinder the electric dipole (ED) is also generated, which creates a radiation pattern directed along the $x = y$ axis when interfering with the magnetic quadrupole. The relative position of the T_d -lattice axes is shown. The cylinder's radius is 140 nm, height is 280 nm, the wavelength is 1480 nm (for ω) and 740 nm (for 2ω), $\epsilon = 12.96$. The width of the truncated cylinder is 230 nm. On the right side the illustration of derivation of the selection rules given by the integral (3) is shown. Cartesian projections of vector spherical harmonics $[\mathbf{N}_\alpha \cdot \mathbf{W}]$ are the scalar functions with particular symmetry which give invariant functions after multiplication.

(\mathbf{N}_{101}) is allowed, and the main part of the radiation energy falls on this mode, which interferes with the magnetic quadrupole, which is reflected in the radiation pattern.

Applying the selection rules to SHG from a magnetic dipole in the cylinder with T_d lattice we obtain that the only non-zero integrals (here we recall the orthogonality properties of vector functions) are $\chi_{zxy}^{(2)} \int_V dV [W_{-1-12n}(2\omega)]_z [M_{-101}(\omega)]_x [M_{-101}(\omega)]_y \propto \chi_{zxy}^{(2)} \int_V dV [\psi_{-12(2z)}][\psi_{-111}][\psi_{111}]$, and for large wavelengths, the main contribution is from $\mathbf{W}_{-1-122} = \mathbf{M}_{-122}$ ($[\mathbf{M}_{-122}]_z = \psi_{-122}$). This integral is illustrated on the right side of fig. 2. In order to allow generation of the electric dipole along z , the integral $\int_V dV [N_{101}(2\omega)]_z [M_{-101}(\omega)]_x [M_{-101}(\omega)]_y \propto \int_V dV (c(r)\psi_{-122} + c'(r)\psi_{-124})$, which is also illustrated on the right side of fig. 2, should contain an invariant, to achieve this, we break the symmetry of the particle by making small cuts along the $x = y$ direction. Since the effect of the appearance of an electric dipole is in violation of symmetry, and it is not associated with resonances, it manifests itself in a range of wavelengths. Moreover, by changing the width of the truncated cylinder, it is possible to control the value of the contribution of the electric dipole. By breaking symmetry along other directions, it is also possible to allow the generation of other dipole (and higher) modes. Note that such cuts also affect the fundamental mode by adding other multipoles to it, but this effect is insignificant and does not affect the selection rules due to the fact that the admixed multipoles have a certain symmetry.

Conclusion. The paper explains the effect of the nanoparticle shape on the second-harmonic signal, and presents a method for finding the selection rules for particles of arbitrary shapes from any non-centrosymmetric material. A table of selection rules for particles of the most common forms is given. The obtained selection rules are also suitable for other nonlinear processes, such as spontaneous parametric scattering, generation of higher harmonics, sum-frequency, etc., with minor changes. Due to the fact that even a slightly imperfect particle shape can significantly affect the generated fields, the results of this work can be used to explain the possible discrepancies between theoretical predictions and experimental observations.

Acknowledgments

The authors thank Petrov M.I., Poddubny A.N., Toftul I.D., Koshelev K.L., Nikolaeva A.A. for the fruitful discussions. The work is supported by the Russian Science Foundation (grant 18-72-10140).

References

1. L. Carletti, A. Locatelli, D. Neshev, and C. De Angelis, "Shaping the Radiation Pattern of Second-Harmonic Generation from AlGaAs Dielectric Nanoantennas," *ACS Photonics* (2016).
2. D. Timbrell, J. W. You, Y. S. Kivshar, and N. C. Panoiu, "A comparative analysis of surface and bulk contributions to second-harmonic generation in centrosymmetric nanoparticles," *Sci. Reports* **8**, 1–9 (2018).
3. S. Wunderlich and U. Peschel, "Plasmonic enhancement of second harmonic generation on metal coated nanoparticles," *Opt. Express* **21**, 18611–18623 (2013).
4. G. Bachelier, I. Russier-Antoine, E. Benichou, C. Jonin, and P.-F. Brevet, "Multipolar second-harmonic generation in noble metal nanoparticles," *J. Opt. Soc. Am. B* **25**, 955–960 (2008).
5. G. D. Bernasconi, J. Butet, and O. J. F. Martin, "Mode analysis of second-harmonic generation in plasmonic nanostructures," *J. Opt. Soc. Am. B* **33**, 768–779 (2016).
6. V. F. Gili, L. Carletti, A. Locatelli, D. Rocco, M. Finazzi, L. Ghirardini, I. Favero, C. Gomez, A. Lemaître, M. Celebrano, C. D. Angelis, and G. Leo, "Monolithic algaas second-harmonic nanoantennas," *Opt. Express* **24**, 15965–15971 (2016).
7. V. N. Kapshai and A. A. Shamyna, "Sum-frequency generation from a thin spherical layer: I. analytical solution," *Opt. Spectrosc.* **124**, 826–833 (2018).
8. L. Carletti, G. Marino, L. Ghirardini, V. F. Gili, D. Rocco, I. Favero, A. Locatelli, A. V. Zayats, M. Celebrano, M. Finazzi, G. Leo, C. De Angelis, and D. N. Neshev, "Nonlinear goniometry by second-harmonic generation in algaas nanoantennas," *ACS Photonics* **5**, 4386–4392 (2018).
9. F. Timpu, A. Sergeyev, N. R. Hendricks, and R. Grange, "Second-harmonic enhancement with Mie resonances in perovskite nanoparticles," *ACS Photonics* **4**, 76–84 (2017).

10. V. B. Novikov, A. A. Nasonov, A. I. Maydykovskiy, and T. V. Murzina, "Enhancement of optical second harmonic generation in hybrid plasmonic-photonic microcavities," *JETP Lett.* **5**, 296–301 (2018).
11. R. Bäümner, L. Bonacina, J. Enderlein, J. Extermann, T. Fricke-Begemann, G. Marowsky, and J.-P. Wolf, "Evanescent-field-induced second harmonic generation by noncentrosymmetric nanoparticles," *Opt. Express* **18**, 23218–23225 (2010).
12. R. Singla and W. L. Mochan, "Analytical Theory of Second Harmonic Generation from a Nanoparticle with a Non-Centrosymmetric Geometry," arXiv:1901.00918 [physics.optics] (2019).
13. R. Czaplicki, J. Mäkitalo, R. Siikanen, H. Husu, J. Lehtolahti, M. Kuittinen, and M. Kauranen, "Second-harmonic generation from metal nanoparticles: Resonance enhancement versus particle geometry," *Nano Lett.* **15**, 530–534 (2015). PMID: 25521745.
14. S. V. Makarov, M. I. Petrov, U. Zywiets, V. A. Milichko, D. A. Zuev, N. Y. Lopanitsyna, A. Y. Kuksin, I. S. Mukhin, G. P. Zograf, E. V. Ubyivovk, D. A. Smirnova, S. V. Starikov, B. N. Chichkov, and Y. S. Kivshar, "Efficient Second-Harmonic Generation in Nanocrystalline Silicon Nanoparticles," *Nano letters* **17**, 3047 (2017).
15. S. A. Scherbak and A. A. Lipovskii, "Understanding the second-harmonic generation enhancement and behavior in metal core-dielectric shell nanoparticles," *The J. Phys. Chem. C* **122**, 15635–15645 (2018).
16. D. A. Smirnova, A. I. Smirnov, and Y. S. Kivshar, "Multipolar second-harmonic generation by Mie-resonant dielectric nanoparticles," *Phys. Rev. A* **97**, 013807 (2018).
17. M. Timofeeva, A. Bouravleuv, G. Cirlin, I. Shtrom, I. Soshnikov, M. Reig Escale, A. Sergeyev, and R. Grange, "Polar second-harmonic imaging to resolve pure and mixed crystal phases along gaas nanowires," *Nano Lett.* **16**, 6290–6297 (2016). PMID: 27657488.
18. O. Wolf, S. Campione, Y. Yang, and I. Brener, "Multipolar second harmonic generation in a symmetric nonlinear metamaterial," *Sci. Reports* (2017).
19. L. Carletti, K. Koshelev, C. De Angelis, and Y. Kivshar, "Giant Nonlinear Response at the Nanoscale Driven by Bound States in the Continuum," *Phys. Rev. Lett.* **121**, 33903 (2018).
20. M. Timofeeva, L. Lang, F. Timpu, C. Renaut, A. Bouravleuv, I. Shtrom, G. Cirlin, and R. Grange, "Anapoles in free-standing iii-v nanodisks enhancing second-harmonic generation," *Nano Lett.* **18**, 3695–3702 (2018). PMID: 29771127.
21. C. F. Bohren and D. R. Huffman, *Absorption and Scattering by a Sphere* (John Wiley and Sons, Ltd, 2007), chap. 4, pp. 82–129.
22. F. Timpu, N. R. Hendricks, M. Petrov, S. Ni, C. Renaut, H. Wolf, L. Isa, Y. Kivshar, and R. Grange, "Enhanced Second-Harmonic Generation from Sequential Capillarity-Assisted Particle Assembly of Hybrid Nanodimers," *Nano Lett.* **17**, 5381–5388 (2017).
23. J. I. Dadap, J. Shan, and T. F. Heinz, "Theory of optical second-harmonic generation from a sphere of centrosymmetric material: small-particle limit," *J. Opt. Soc. Am. B* **21**, 1328–1347 (2004).
24. M. Finazzi, P. Biagioni, M. Celebrano, and L. Duò, "Selection rules for second-harmonic generation in nanoparticles," *Phys. Rev. B* **76**, 125414 (2007).
25. J. A. Stratton, *Spherical Waves* (John Wiley & Sons, Ltd, 2015), chap. VII, pp. 392–423.
26. X. G. Santiago, M. Hammerschmidt, S. Burger, C. Rockstuhl, I. Fernandez-Corbaton, and L. Zschiedrich, "Decomposition of scattered electromagnetic fields into vector spherical wave functions on surfaces with general shapes," *Phys. Rev. B* **99**, 045406 (2019).
27. E. C. Le Ru, W. R. Somerville, and B. Auguie, "Radiative correction in approximate treatments of electromagnetic scattering by point and body scatterers," *Phys. Rev. A - At. Mol. Opt. Phys.* (2013).
28. K. G. Kulikov, "Light scattering by dielectric bodies of irregular shape in a layered medium in problems of biomedical optics: I. theory and computational model," *Tech. Phys.* **57**, 1623–1631 (2012).
29. K. Frizyuk, I. Volkovskaya, D. Smirnova, A. Poddubny, and M. Petrov, "Second-harmonic generation in mie-resonant dielectric nanoparticles made of noncentrosymmetric materials," *Phys. Rev. B* **99**, 075425 (2019).
30. L.-W. L. P.-S. K. M.-S. L. T.-S. Yee; and P.-s. Kooi, "Electromagnetic Dyadic Green's Function in Spherically Multilayered Media," *Microw. Theory Tech. IEEE Transactions on* (1994).
31. C. T. Tai and C. Yeh, "Dyadic Green's Functions in Electromagnetic Theory," (1972).
32. M. B. Doost, W. Langbein, and E. A. Muljarov, "Resonant-state expansion applied to three-dimensional open optical systems," *Phys. Rev. A - At. Mol. Opt. Phys.* (2014).
33. N. A. Loiko, A. A. Miskevich, and V. A. Loiko, "Scattering of polarized and natural light by a monolayer of spherical homogeneous spatially ordered particles under normal illumination," *Opt. Spectrosc.* **125**, 655–666 (2018).
34. L. Carletti, G. Marino, L. Ghirardini, V. F. Gili, D. Rocco, I. Favero, A. Locatelli, A. V. Zayats, M. Celebrano, M. Finazzi, G. Leo, C. De Angelis, and D. N. Neshev, "Nonlinear goniometry by second-harmonic generation in algaas nanoantennas," *ACS Photonics* **5**, 4386–4392 (2018).
35. L. Landau and E. Lifshitz, "Chapter xii - the theory of symmetry," in *Quantum Mechanics (Third Edition)*, (Pergamon, 1977), pp. 354 – 395.
36. H. Zhang and Y. Han, "Addition theorem for the spherical vector wave functions and its application to the beam shape coefficients," *J. Opt. Soc. Am. B* **25**, 255–260 (2008).
37. D. A. Varshalovich, A. N. Moskalev, and V. K. Khersonsky, *Quantum Theory of Angular Momentum: Irreducible Tensors, Spherical Harmonics, Vector Coupling Coefficients, 3nj Symbols* (World Scientific, Singapore, 1988).
38. S. H. Dong and R. Lemus, "The overlap integral of three associated Legendre polynomials," *Appl. Math. Lett.* **15**,

- 541–546 (2002).
39. S. Wunderlich, “Second harmonic light scattering from dielectric and metallic spherical nanoparticles,” doctoralthesis, Friedrich-Alexander-Universität Erlangen-Nürnberg (FAU) (2014).
 40. S. S. Kruk, R. Camacho-Morales, L. Xu, M. Rahmani, D. A. Smirnova, L. Wang, H. H. Tan, C. Jagadish, D. N. Neshev, and Y. S. Kivshar, “Nonlinear optical magnetism revealed by second-harmonic generation in nanoantennas,” *Nano Lett.* **17**, 3914–3918 (2017). PMID: 28511012.
 41. R. Camacho-Morales, M. Rahmani, S. Kruk, L. Wang, L. Xu, D. A. Smirnova, A. S. Solntsev, A. Miroshnichenko, H. H. Tan, F. Karouta, S. Naureen, K. Vora, L. Carletti, C. De Angelis, C. Jagadish, Y. S. Kivshar, and D. N. Neshev, “Nonlinear generation of vector beams from algaas nanoantennas,” *Nano Lett.* **16**, 7191–7197 (2016). PMID: 27797212.
 42. L. Ghirardini, L. Carletti, V. Gili, G. Pellegrini, L. Duò, M. Finazzi, D. Rocco, A. Locatelli, C. D. Angelis, I. Favero, M. Ravaro, G. Leo, A. Lemaître, and M. Celebrano, “Polarization properties of second-harmonic generation in algaas optical nanoantennas,” *Opt. Lett.* **42**, 559–562 (2017).
 43. M. Guasoni, L. Carletti, D. Neshev, and C. De Angelis, “Theoretical model for pattern engineering of harmonic generation in all-dielectric nanoantennas,” *IEEE J. Quantum Electron.* **53**, 1–5 (2017).
 44. S. Hayami, M. Yatsushiro, Y. Yanagi, and H. Kusunose, “Classification of atomic-scale multipoles under crystallographic point groups and application to linear response tensors,” *Phys. Rev. B* **98**, 165110 (2018).
 45. T. Das, P. P. Iyer, R. A. DeCrescent, and J. A. Schuller, “Beam engineering for selective and enhanced coupling to multipolar resonances,” *Phys. Rev. B* **92**, 241110 (2015).
 46. E. V. Melik-Gaykazyan, S. S. Kruk, R. Camacho-Morales, L. Xu, M. Rahmani, K. Zangeneh K., A. Lamprianidis, A. E. Miroshnichenko, A. A. Fedyanin, D. N. Neshev, and Y. S. Kivshar, “Selective Third-Harmonic Generation by Structured Light in Mie-Resonant Nanoparticles,” *ACS Photonics* **5**, 728–733 (2018).
 47. E. V. Melik-Gaykazyan, K. L. Koshelev, J.-H. Choi, S. S. Kruk, H.-G. Park, A. A. Fedyanin, and Y. S. Kivshar, “Enhanced second-harmonic generation with structured light in algaas nanoparticles governed by magnetic response,” *JETP Lett.* (2019).

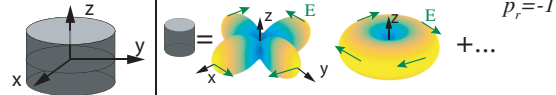
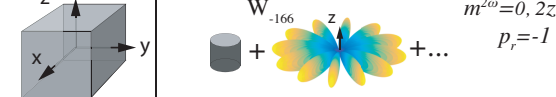
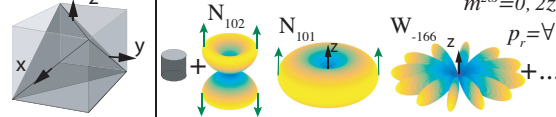
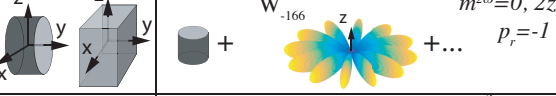
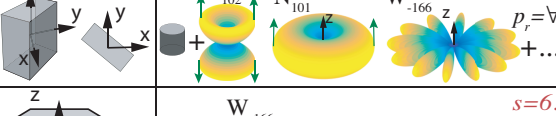
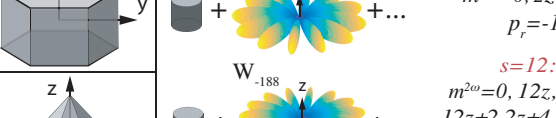
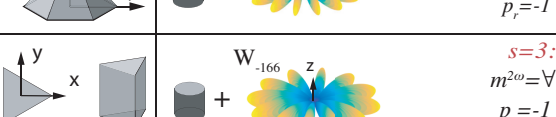
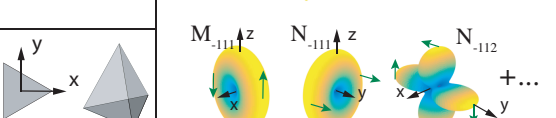
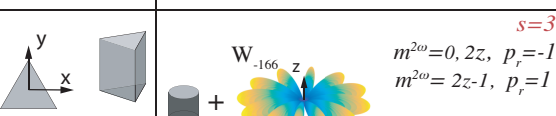
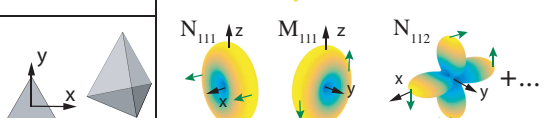
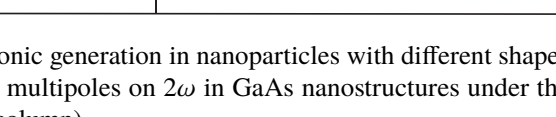
Particle symmetry, and functions, which contain invariant. $z \in \mathbb{Z}, k \in \mathbb{Z}$	Selection rules			Plane wave:  T_d structure: 
	1.	2.	3.	
Vertical cylinder $\psi_{10}(2z)$	0	1	-1	
Cube (O_h) $\psi_{e00}, \psi_{e(4z)(2k)}, k \geq 2$ [44]	$\div 4$	1	-1	
Tetrahedron (T_d) $\psi_{e00}, \psi_{e(4z)(2k)}, k \geq 2$ ψ_{-123} , [44]	$\div 4$	1	-1	
	$\nexists 4, \div 4z-2$	-1	1	
Rotated cylinder, rectangular prism $\psi_{1(2k)}(2z)$	$\div 2$	1	-1	
Rotated rectangular prism (or cylinder) $\psi_{1(4k)}(2z)$ $\psi_{-1(4k-2)}(2z)$	$\div 4$	1	-1	
	$\nexists 4, \div 4z-2$	-1	-1	
s-gonal prism, even s $\psi_{10}(2z), \psi_{1(s \cdot z)}(2k)$	$\div s$	1	-1	
s-gonal pyramid, even s $\psi_{10n}, \psi_{1(s \cdot z)n}$	$\div s$	1	\forall	
s-gonal prism, odd s, symmetry under $y \rightarrow -y$ $\psi_{10}(2z), \psi_{1(s \cdot 2z)}(2k)$ $\psi_{1(s \cdot (2z-1))}(2k-1)$	$\div s, \div 2$	1	-1	
	$\div s, \nexists 2$	1	1	
s-gonal pyramid, odd s, symmetry under $y \rightarrow -y$ $\psi_{10n}, \psi_{1(s \cdot z)n}$	$\div s$	1	\forall	
s-gonal prism, odd s, symmetry under $x \rightarrow -x$ $\psi_{10}(2z), \psi_{1(s \cdot 2z)}(2k)$ $\psi_{-1(s \cdot (2z-1))}(2k-1)$	$\div s, \div 2$	1	-1	
	$\div s, \nexists 2$	-1	1	
s-gonal pyramid, odd s, symmetry under $x \rightarrow -x$ $\psi_{10n}, \psi_{1(s \cdot 2z)n}$ $\psi_{-1(s \cdot (2z-1))n}$	$\div s, \div 2$	1	\forall	

Table 1. Selection rules for second harmonic generation in nanoparticles with different shapes (left columns), and examples of allowed multipoles on 2ω in GaAs nanostructures under the x-polarized plane-wave excitation (right column).